JOURNAL OF GEOPHYSICAL RESEARCH, VOL. 96, SUPPLEMENT, PAGES 19,187–19,196, OCTOBER 30, 1991

Dust Distribution Around Neptune: Grain Impacts Near the Ring Plane Measured by the Voyager Planetary Radio Astronomy Experiment

B. M. PEDERSEN, N. MEYER-VERNET, M. G. AUBIER,[1] AND P. ZARKA

Observatoire de Paris-Meudon, France

During the Voyager 2 flyby of Neptune the planetary radio astronomy (PRA) experiment recorded an intense noise near the equatorial plane around 3.4 and 4.2 R_N, as already observed during previous Voyager ring plane crossings at Saturn and Uranus. This noise is interpreted as being due to impact ionization of dust grains striking the spacecraft. We deduce a power law index of the grain mass distribution of about 2. The PRA system is sensitive to particles with radii larger than $\sim$1.6 μm, and the largest particles, detected near the ring plane, are evaluated to have a radius of $\sim$10 μm. The spatial dust distribution along the spacecraft trajectory around the two equatorial crossings is found not to be symmetrical with respect to the ring plane and spread over wide regions: over $\sim$2 R_N perpendicularly to the equatorial plane with the densest part concentrated within $\sim$700 km. The vertical optical depth τ of this dense region is found to be $10^{-6} - 10^{-8}$.

1. INTRODUCTION

During the Neptune flyby on August 25 (day of year (DOY) 237), 1989, Voyager 2 passed through the ring plane of the planet twice. During the inbound pass, the ring plane was crossed at about 0253 UT spacecraft event time (SCET) at a distance of $\sim$3.4 Neptunian radii (R_N) from the center of the planet. The outbound crossing took place on the way toward Triton at about 0515 SCET at a distance of $\sim$4.2 R_N.

During both crossings the planetary radio astronomy experiment (PRA) detected an intense unpolarized, broadband noise [*Warwick et al.*, 1989]. As for the previous ring plane crossings at Saturn [*Aubier et al.*, 1983] and at Uranus [*Meyer-Vernet et al.*, 1986, hereafter referred to as paper 1], we interpret this noise as being due to dust grains impacting the spacecraft, then being vaporized and ionized, and eventually recollected by the spacecraft structures. This causes impulsive variations of the spacecraft potential, giving rise to the observed noise. These impacts were also recorded by the Voyager plasma wave instrument [*Gurnett et al.*, 1989]. This instrument, working at lower frequencies, can detect larger spectral levels which, however, in opposition to the response of the PRA receiver, may be more difficult to interpret because they are not evaluated with respect to the spacecraft potential.

In this article we detail the ring plane PRA observations (section 2) from the 6-s scan routine mode and relate them to high-rate mode data, recorded immediately before the outbound ring plane passage, as previously reported by *Warwick et al.* [1989]. Section 3 develops our theoretical interpretation of ring plane noise. A comparison of the routine mode observations with calculated power spectra gives an estimate of parameters of the grain mass distribution around the Neptunian ring plane (section 4.1). By using high-rate data we evaluate the power law mass distribution of the grains (section 4.2). This allows us to determine the number density of grains in the vicinity of the ring plane at the time of the crossings (section 4.3). We analyze in section 4.4 the spatial dust distribution along the spacecraft trajectory around the two ring plane passages. Finally, we discuss the reliability of our results.

2. PRA OBSERVATIONS

The receiving system, described in detail by *Warwick et al.* [1977], consists of a pair of 10-m orthogonal monopoles, loaded against the conductive structure of the satellite and connected to a high-sensitivity broadband receiver (1.2 kHz to 40.2 MHz).

2.1. *The 6-s Scan Routine Observations*

The basic (routine) mode, originally designed to obtain dynamic spectra of the electric field flux density of planetary radio emissions, sweeps through the total frequency range each 6 s, dwelling $\Delta t = 25$ ms at each of 198 channels and measuring alternately flux densities of right- and left-hand circular polarizations. For successive scans the order of polarization measurements is inverted, thus giving one point of measurement with same polarization for each frequency channel every 12 s. The 198 channels of the swept frequency receiver are grouped in two frequency bands: (1) the high-frequency (HF) band, containing 128 channels with 200-kHz bandwidth and uniformly spaced from 40.2 MHz to 1228 kHz, and (2) the low-frequency (LF) band, covering 70 channels with 1-kHz bandwidth, uniformly spaced (19.2 kHz apart) from 1326 to 1.2 kHz.

Figure 1 displays the emissions, associated with the two ring plane crossings, within the context of the PRA observations during closest approach to Neptune [*Warwick et al.*, 1989]. Below $\sim$800 kHz the ring plane emissions are superimposed on the nonthermal planetary radio emission, the so-called Neptunian kilometric radiation. In this figure, only frequency channels from the LF band have been shown. At both crossings the signature of the ring plane noise extended into the HF band where, however, the data are not usable due to instrumental problems.

The 6-s scan mode data detected at the time of the inbound ring plane crossing around 0253 SCET are presented in Figure 2. Data gaps immediately before and

[1]Also at Université de Paris VI, France.

Paper number 91JA01601.
0148-0227/91/91JA-01601$05.00

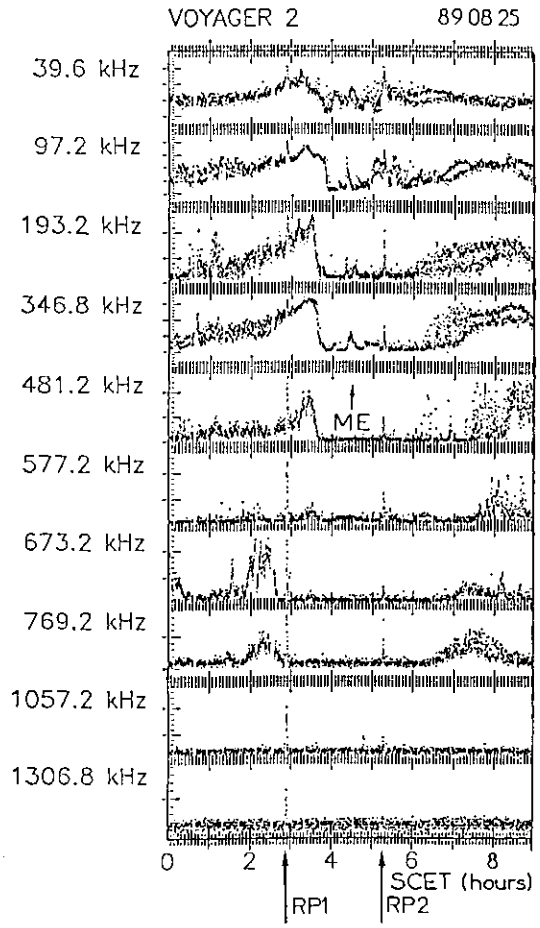

Fig. 1. Relative intensity plots of 10 PRA fixed frequency channels, as a function of time during an interval of 9 hours around the ring plane crossings: RP1 (inbound) and RP2 (outbound). The emissions (detailed in Figures 2 and 3) are of short duration and superimposed on the Neptunian kilometric radiation (NKR) at low frequencies. Note another short emission peak at the crossing of the hypothetic magnetic equator (ME) for the offset tilted magnetic dipole model.

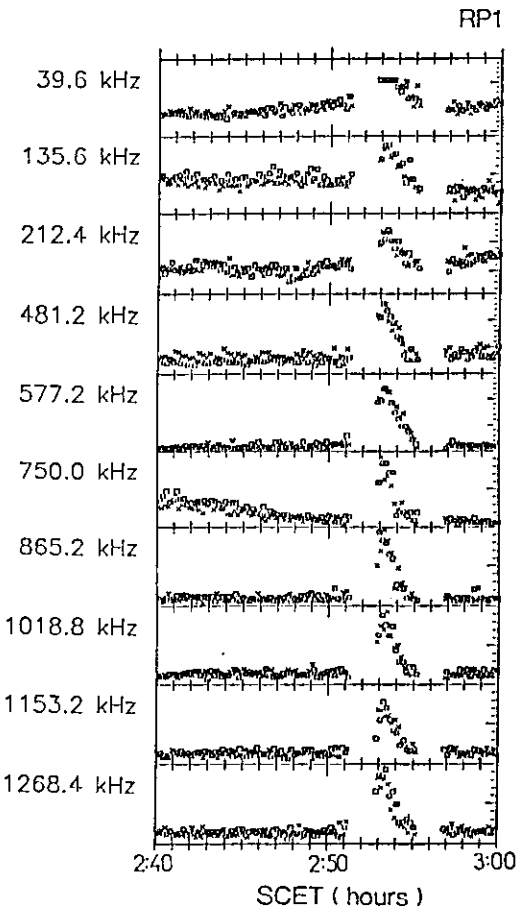

Fig. 2. Relative intensity plots of 10 PRA fixed frequency channels, as a function of time during 20 min around the inbound ring plane crossing (RP1 at about 0253:20 SCET). The symbols refer to the measurements of circular polarizations (left- and right-hand are shown by squares and crosses, respectively). Channel 39.6 kHz (as well as 1.2 and 20.4 kHz) is saturated during this ring plane crossing. Vertical white areas immediately before and after the crossing are data gaps for the 6-s scan routine mode.

after the passage are due to other mode options (cf. section 2.2). The associated noise is extremely intense, in fact one of the strongest ever recorded by this instrument. This is due to higher relative grain–spacecraft velocities v at the time of the ring plane crossings compared to the previous Voyager encounters. Indeed, as we shall see below (section 3.1 , equations (3) and (4)), the induced electric power, being a function of both the impact rate ($N \propto v$) and the square of the total charge released by each impacting grain ($Q \propto v^{3.5}$), is proportional to v^8. This ring plane passage may have caused some damage to our instrument, which since that time has operated with new, until then not observed, interferences (visible as vertical streaks in Figure 3*a*). But since other experiments on board Voyager 2 have also behaved abnormally after the first passage, it might also be due to a slight deterioration of the flight data subsystem.

The routine mode observations around the outbound ring plane crossing at ~0515 SCET are represented in Figures 3*a* and 3*b*, displaying the dynamic spectrum of the entire LF band (Figure 3*a*) and selected channels (Figure 3*b*). The extension in time of the ring plane noise phenomenon toward lower frequencies is clearly visible. In fact, the Voyager plasma wave instrument [*Gurnett et al.*, 1989] observes at frequencies below the PRA range a slowly increasing noise during several hours before and after the crossings.

Figure 4 presents the spectral density at the time when it is maximum during the two ring plane crossings. In both cases the noise saturates the lowest-frequency channels of the receiver. For every passage the slope of the line that best fits the data points indicates an approximate frequency dependence f^{-1}, as already obtained for similar events at Saturn [*Aubier et al.*, 1983] and Uranus (paper 1).

2.2. *High Rate Mode Observations*

The PRA experiment can be operated in a special high-rate mode, designed for high time resolution, fixed-frequency observations. The high-rate operation is functional only at selected times. Since using this mode requires an important part of the telemetry capacity of the spacecraft and it is executed at the expense of the imaging experiment, very few observations have been performed during each planetary encounter.

Around Neptune, this mode was executed in the following way: two channels, with a bandwidth of 200 kHz and separated by 307.2 kHz, were sampled alternately with opposite states of polarization during a PRA frame

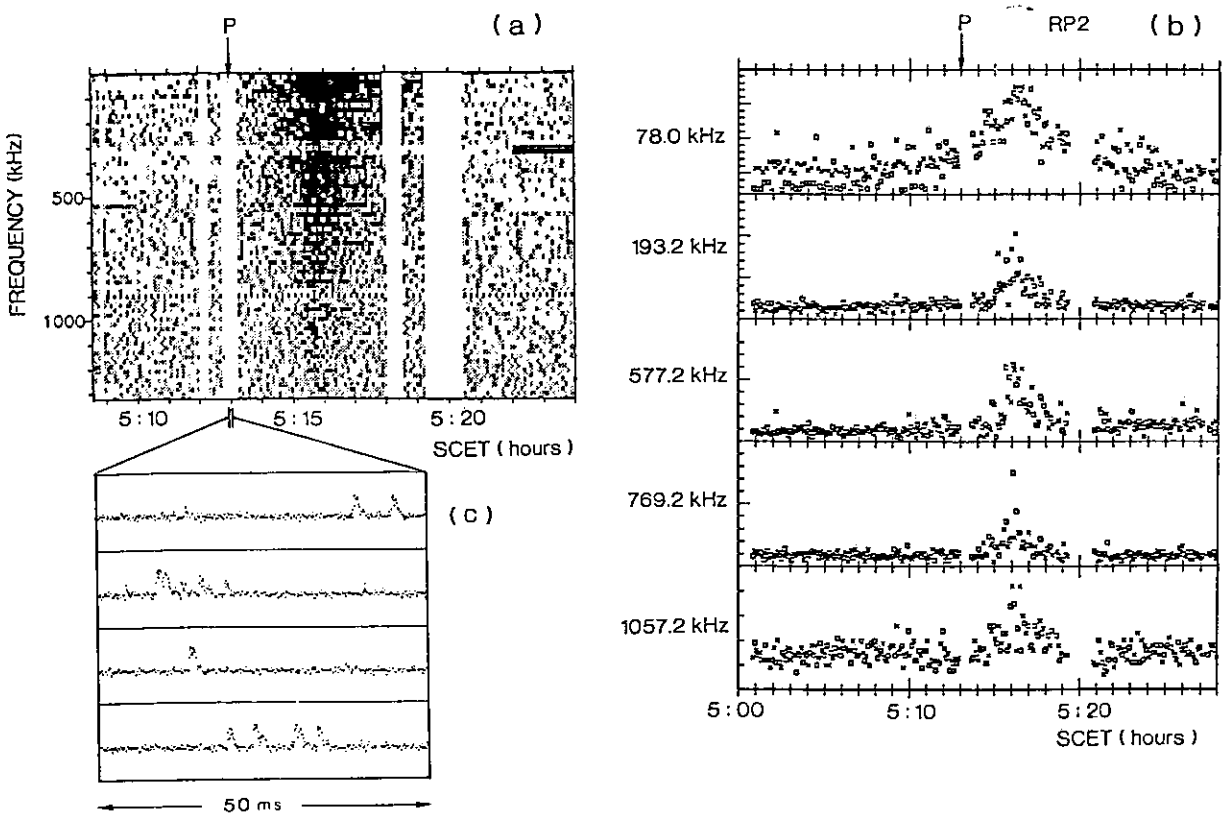

Fig. 3. Observations during 30 min around the outbound ring plane crossing (RP2 at about 0516 SCET). (*a*) Dynamic spectrum of the PRA LF band. Horizontal lines and vertical streaks are due to spacecraft interferences. Vertical white areas are data gaps for the 6-s scan mode. (*b*) Relative intensity plots of five fixed frequencies in LF band. Symbols for polarization as in Figure 2. (*c*) Extracts of high-rate data, acquired during the routine data gap P, indicated in Figures 3*a* and 3*b*. Each line represents nonconsecutive 50-ms intervals of observations at 615.6 kHz, one of the two selected channels. The total intensity range is 70 dB.

(48 s). For each of the two selected frequencies, one point is acquired every 140 μs with an integration time $\Delta t_{hr} = 100$ μs [*Warwick et al.*, 1989].

Several frames of the high-rate mode were acquired around each of the two ring plane crossings. Figure 3c presents four nonconsecutive intervals of 50 ms from the 615.6-kHz channel, which together with the 308.4-kHz channel were recorded a few minutes before entering the densest part associated with the outbound ring plane crossing (indicated by P in Figures 3*a* and 3*b*). This figure shows clearly individual impacts, occasioning different potential changes of the spacecraft. The average impact rate during the entire data frame observed during "P" is found to be $N_o \sim 65$ s^{-1}, when taking into account the impacts causing intensity level increases greater than σ, the average variation of the noise level. In section 4.2 we shall discuss the statistics of the impact intensities.

3. Electric Antennae as Dust Detectors

The first question we have to answer is whether the noise observed near the ring plane can be due to the ambient plasma particles, namely, the thermal noise or the shot noise of impacting electrons and ions. With an electron density, $n \approx 0.004$ cm^{-3} and $n \approx 0.05$ cm^{-3} at the first and second ring plane crossing respectively, and a temperature around $T \approx 6$ eV, which are preliminary estimates (Voyager Plasma Science Experiment, private communication, 1990), we find, using the formulae of *Meyer-Vernet and Perche* [1989], noise levels at least 3 orders of magnitude smaller than the observed values.

Let us now calculate the noise due to a population of small dust grains. When a grain impinges on the spacecraft or its antennae with a high velocity, it is vaporized and ionized. This produces an expanding plasma cloud with a charge separation, and a fraction of the released charge is eventually re-collected by the antennae or the spacecraft. This process produces a time variation of the voltage, which is detected by the receiver.

The charge released upon impact is typically much larger than the electrostatic charge normally carried by a grain, so that the detected potential is generally much larger than that induced by a grain which passes near the spacecraft without impacting it. It is important to note, however, that the latter events are much more numerous than the impacts, so that the passing grains might dominate the observations when the grain number density is so small that impacts are very rare [*Lesceux et al.*, 1989].

For estimating parameters of the impacting grains, we will proceed essentially as in paper 1 but also use informations obtained with a few high-rate data.

3.1. *Noise Due to Impacts of Identical Grains*

Let us first assume arbitrarily that all the grains have the same mass m, and impacting velocity v. We will later generalize to a continuous mass distribution. Each impact produces a time variation of the antenna voltage

$V(t)$. If the impacts are independent, with an impact rate N, this produces a noise power spectrum (for a stationary process)

$$V^2 = 2N|V(\omega)|^2 \quad (1)$$

where $V(\omega)$ is the Fourier transform of the voltage variation $V(t)$.

The impact rate N can be expressed as a function of the surface of the target $S_\perp$ projected normally to the velocity v, and of the grain number density n_G as

$$N = n_G \; v \; S_\perp \quad (2)$$

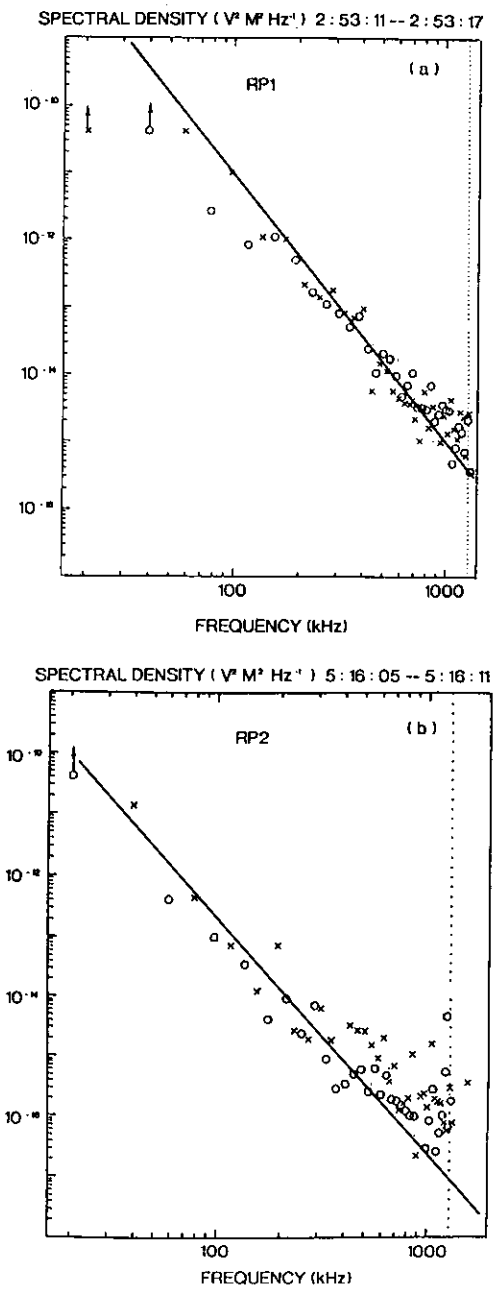

Fig. 4. The electric field spectra observed at the two ring plane crossings: (*a*) inbound and (*b*) outbound. The points represent the noise peak levels for each frequency channel during the PRA scan at the time of maximum intensity. Arrows indicate levels of saturated channels. These points are to be compared with the derived theoretical values (inserted lines with a f^{-4} slope) for each event (equations (16) and (17)).

The two PRA antennae are monopoles, responding to the difference of potential between the antenna and the spacecraft structure. The relevant target surface for impacts is therefore both the antennae and the spacecraft. However, compared to the projected surface of the spacecraft that of the antennae is negligible. When a fraction of the charge released by an impacting grain, say, Q, is re-collected by the spacecraft (or by the antennae), the measured voltage $V(t)$ increases up to the maximum value

$$V = Q/C_0$$

C_0 being the capacitance between a monopole and the spacecraft. We take as in paper 1 $C_0 \approx 2 \times 80$ pF, which includes the base capacitance. This figure is based on measurements, using a reduced model of the Voyager spacecraft and its radio astronomy antennae (G. Daigne, private communication, 1986). Note that this detection in monopole mode is much more favorable than the usual dipole mode used in most experiments: in the latter case the receiver only detects the difference of potential between the two antenna arms, so that it is not sensitive to any charge re-collected by the spacecraft except through the small dissymmetry of the system.

Now we have to evaluate the charge Q and the form of the time variation of the induced potential $V(t)$. This is a very difficult problem: one would have to study the vaporization and ionization of both the grain and target material upon impact, the dynamics of the produced plasma cloud, its charge separation, and the corresponding electric field, taking also the ambient plasma into account; all must be done in the context of the actual complicated geometry of the system. For dust impact detectors, which are much simpler, this is usually solved empirically by using laboratory measurements.

But an important problem with the Voyager spacecraft is that the surface exposed to dust impacts is made of different materials. Most of the spacecraft surface is covered with thermal blankets, i.e., black carbon cloth, which is a woven material made of a composite of fiberglass/polyimide plastics containing carbon trapped in the fibers. The large telemetry antenna, which represents most of the surface, is made of a not very different material: graphite epoxy with an additional overcoat (M. H. Acuna, private communication, 1991). The response of these kinds of materials to dust impacts is not well known. In fact, even if it had been measured in the laboratory, the results might be irrelevant because they are very dependent on the nature of the impacting material, which is unknown; in addition, since it is difficult to accelerate large grains to high velocities, the laboratory results generally concern grains much smaller than those relevant here.

The problem may be eluded by noting that the radio antennae (made of BeCu) with a total projected surface of about 1/30 of that of the spacecraft (including the large telemetry antenna) should have a rather high yield. Thus we shall assume that all the relevant surfaces have a typical "laboratory" yield, as has been measured for metallic targets, and remember that, even if the spacecraft structure (plus telemetry antenna) had a negligible yield to dust impacts, which is possible, this would change our results (which are proportional to the total target's surface) by about a factor of 30. We will therefore use the same estimate as in paper 1,

$$Q = Q_0 m^\alpha v^\beta \quad (3)$$

with $\beta \approx 3.5$, $\alpha \approx 0.8$ and $Q_0 \approx 2 \times 10^{-7}$, Q in coulombs, m in grams and v in kilometers per second. This is 2 times below an empirical formula deduced for dust detectors. Indeed, as discussed by *Kruger and Kissel* [1984], the released charge Q does not vary simply as the grain kinetic energy (mv^2) as one would naively expect. In particular, the value $\alpha \approx 1$ (i.e., $Q \propto m$), often used, mostly holds for very small grains for which both electron recombination and surface phenomena are negligible. The exact value of α is somewhat controversial, but it is not crucial here, because, as we will see later, we are concerned with a rather limited range of grain size. For solid spherical icy grains of radius $a = 1$ μm ($m \approx 4 \times 10^{-12}$ g) we get with (3), Q/m (C/g) $\approx 4 \times 10^{-5} v^{3.5}$ (v in kilometers per second) and a value only 4 times smaller for $a = 10$ μm; these values are in the range of recent laboratory measurements with gold targets [*Göller and Grün*, 1989].

As in our previous papers, we approximate the signal $V(t)$ as having a rise time τ_r and a decay time τ_d (of the order of the time constant of the system RC_0) with $\tau_d \gg \tau_r$. For frequencies $f \gg 1/2\pi\tau_r$ the electric field power spectrum stems from the rise part of the signal, which gives

$$E^2 = V^2/L^2 \approx 2NQ^2/C_0^2\tau_r^2\omega^4 L^2 \qquad (4)$$

where L is the antenna equivalent length $L = 7$ m.

Note that at lower frequencies satisfying $1/2\pi\tau_d \ll f \ll 1/2\pi\tau_r$ (i.e., most of the frequency range of the Voyager plasma wave experiment [*Gurnett et al.*, 1989]), this would yield a f^{-2} spectrum, since in this case, (4) must be multiplied by the factor $\omega^2\tau_r^2$ [*Aubier et al.*, 1983]. On the basis of physical considerations and laboratory measurements the rise time is expected to range from about 10 to 100 μs. The fact that the observed spectrum varies as f^{-1} at least for frequencies $f > 40$ kHz indicates that $\tau_r > 5$ μs; since the receiver is saturated at smaller frequencies, we cannot get a stronger limit. For the ring plane crossing at Uranus the same constraint gave $\tau_r > 10$ μs, and the plasma wave instrument [*Gurnett et al.*, 1987] observed a rise time of the order of of 30 μs corresponding to the upper cutoff frequency of this receiver, implying $\tau_r \leq 30$ μs, with an impact velocity somewhat smaller than the present one. Thus, as we did previously, we use the very rough estimate $\tau_r \approx 20$ μs, consistent with the constraints of the physical system (paper 1).

We now have to determine the relative velocity v and the projected surface $S_\perp$ of the target. Using the spacecraft trajectory and attitude data for the Neptune encounter and assuming that the grains revolve in direct equatorial orbits, we find for the inbound and outbound ring plane crossings $v \approx 24$ and 23 km/s, respectively, with angles ϕ of 30° and 46° with respect to the Z axis of the spacecraft (s/c–Z axis). From (3) we deduce the approximate charge released upon impact for both ring plane passages,

$$Q \approx q\, m^{0.8} \approx 0.013\, m^{0.8} \qquad (5)$$

(equivalent to 2.5 C/g for 1 μm grains). The relatively small angles between the velocity and the s/c–Z axis mean that the large ($D \approx 3.7$ m diameter) telemetry antenna cannot be neglected when calculating the target projected surface. So to the approximate projected spacecraft surface of ~ 2 m^2 we have to add the projected antenna areas $\cos\phi \times \pi D^2/4 \approx 9.3$ and 7.4 m^2, respectively, for the two encounters. In view of the uncertainties concerning the relevant surfaces and their response to dust impacts we take for both ring plane passages the same approximate value of $S_\perp \approx 10$ m^2. Note that laboratory measurements indicate that the released charge Q does not vary too much with the incidence angle of the impinging particles [*Göller and Grün*, 1989].

With these parameters we get for the impact rate N (per second) as a function of the grain number density n_G (in units per cubic meter)

$$N = n_G\, v\, S_\perp \approx 2.3 \times 10^5 n_G \qquad (6)$$

Substituting (5) into (4), the theoretical power spectrum reads

$$E^2 \approx 2q^2 N m^{1.6}/L^2 C_0^2 \tau_r^2 (2\pi f)^4 \qquad (7)$$

$$E^2 \approx 2q^2 v S_\perp n_G m^{1.6}/L^2 C_0^2 \tau_r^2 (2\pi f)^4 \approx 10^{26} n_G m^{1.6}/f^4 \qquad (8)$$

with E^2 in $V^2\ m^{-2}\ Hz^{-1}$, the frequency f in hertz, and the mass m in grams.

Since the high–rate mode data (see section 4.2) indicate that the particles are not identical, we shall integrate the above equations over the particle mass distribution.

3.2. *Continuous Mass Distribution*

Let us now assume that the impacting grains have a continuous mass distribution of the form

$$\frac{dn_G}{dm} = Am^{-p} \qquad (9)$$

with n_G in units per cubic meter and m in grams. Note that p is related to the exponent of a size distribution $dn_G/da \propto a^{-q}$, by $p = (q+2)/3$. We assume, as in paper 1, that

$$1 < p < 2.6$$

Indeed, many physical systems have p of the order of 1 or slightly larger; interplanetary grains at 1 AU have $p \approx 1.4$ in the mass range $10^{-14} < m < 10^{-9}$ g [*Grün et al.*, 1985]; small collisional ejecta have $p \sim 1.8$. An exception is the very high value $p = 3$ found at Saturn's ring plane crossing by the Voyager plasma wave experiment [*Gurnett et al.*, 1983]. However, we find this result very questionable: it does not take into account the fact that large grains ($m > m_2$; cf. (12) below) do not contribute to the voltage, as the probability that they impact the target in the finite measurement time is negligible. Furthermore, m_2 also depends on the grain number density. Note that the measurements of *Gurnett et al.* [1983] present a calibration error, due to a confusion between dipole and monopole mode. This has tentatively been corrected in a subsequent paper [*Gurnett et al.*, 1987] by using the comparison with the PRA measurements from paper 1 as a calibration.

With the continuous distribution (9) we get, as in paper 1, for the impact rate and power spectrum, instead of (6) and (8), respectively,

$$N = vS_\perp \int_{m_1}^{m_2} \frac{dn_G}{dm} dm \approx \frac{vS_\perp A}{(p-1)\, m_1^{p-1}} \qquad (10)$$

with $vS_\perp \approx 2.3\times10^5$ and

$$E^2 \approx \frac{2q^2vS_\perp}{L^2C_0^2\tau_r^2(2\pi f)^4}\int_{m_1}^{m_2}\frac{dn_G}{dm}m^{1.6}dm \approx \frac{2q^2vS_\perp}{L^2C_0^2\tau_r^2(2\pi f)^4}\frac{Am_2^{2.6-p}}{2.6-p} \approx \frac{10^{26}}{f^4}\frac{Am_2^{2.6-p}}{2.6-p} \quad (11)$$

where we have substituted $\tau_r \approx 20$ μs. Here m_1 and m_2 are the smallest and largest detected masses, respectively, assuming $m_1 \ll m_2$. We see that with our plausible assumption $1 < p < 2.6$ the voltage is sensitive to the largest grains, while the impact rate is sensitive to the smallest ones. (Note also that we have neglected a possible variation of the rise time τ_r with the grain mass.)

Now we can obtain a broad estimate of the largest detected mass m_2 , which stems from the finite individual measurement time Δt. As in paper 1 (writing that the probability of having one impact with $m > m_2$ is about $1/e$, with a Poisson statistic) we have

$$vS_\perp\int_{m_2}^{\infty}\frac{dn_G}{dm}dm \sim 1/\Delta t \quad (12)$$

Thus with $\Delta t = 0.025$ s, which is the dwelling time in the routine mode,

$$\frac{A}{(p-1)m_2^{p-1}} \approx \frac{1}{vS_\perp\Delta t} \approx 1.7\times10^{-4} \quad (13)$$

so that, eliminating A, (11) reads

$$E^2 \approx \frac{2q^2}{\Delta t L^2C_0^2\tau_r^2(2\pi f)^4}m_2^{1.6}\frac{p-1}{2.6-p} \quad (14)$$

$$E^2 \approx \frac{1.6\times10^{22}}{f^4}m_2^{1.6}\frac{p-1}{2.6-p} \quad (15)$$

4. DEDUCING GRAIN PARAMETERS

From the above calculations, what can be deduced about the characteristics of the grains? Routine measurements (section 2.1) and high–rate data (section 2.2) provide complementary information.

4.1. *Using 6–s scan routine data*

As illustrated in Figure 4, the power spectra obtained around the two ring plane crossings, inbound at $\sim$3.45 R_N (85,400 km) and outbound at $\sim$4.26 R_N (105,500 km), are at their time of maximum

inbound (3.45 R_N)

$$E^2 \approx 10^9/f^4 \quad (16)$$

outbound (4.26 R_N)

$$E^2 \approx 2\times10^7/f^4 \quad (17)$$

Equating these values with the theoretical power spectrum (14), we get the maximum detected mass (in grams)

$$m_2 \approx \left(\frac{E^2\Delta tL^2C_0^2\tau_r^2(2\pi f)^4}{2q^2}\frac{2.6-p}{p-1}\right)^{1.6} \quad (18)$$

thus

inbound (3.45 R_N)

$$m_2 \approx 5.6\times10^{-9}\left(\frac{2.6-p}{p-1}\right)^{1/1.6} \quad (19)$$

outbound (4.26 R_N)

$$m_2 \approx 4.8\times10^{-10}\left(\frac{2.6-p}{p-1}\right)^{1.6} \quad (20)$$

From (12) the number density (in units per cubic meter) of grains larger than m_2 (in grams) is

$$n_{G>m_2} \approx 1/(vS_\perp\Delta t) \approx 1.7\times10^{-4} \quad (21)$$

Hence with (9) and (21) we get for the number density of grains larger than a given mass m

$$n_{G>m} = n_{G>m_2}(m_2/m)^{p-1} \approx 1.7\times10^{-4}(m_2/m)^{p-1} \quad (22)$$

Now we need a determination of the exponent p of the distribution in order to deduce m_2 from (19) and (20) and thus the grain number density for a given mass (or, equivalently, to deduce the parameter A of the distribution). Note, however, that m_2 generally does not depend very much on the exponent p.

With $p = 1.5$ we get for the maximum detected mass and radius (assuming solid water ice spheres)

inbound

$$m_2 \approx 9\times10^{-9}\text{ g} \qquad a_2 \approx 13\ \mu m \quad (23)$$

outbound

$$m_2 \approx 0.8\times10^{-9}\text{ g} \qquad a_2 \approx 6\ \mu m \quad (24)$$

With $p = 2$, we get

inbound

$$m_2 \approx 4\times10^{-9}\text{ g} \qquad a_2 \approx 10\ \mu m \quad (25)$$

outbound

$$m_2 \approx 4\times10^{-10}\text{ g} \qquad a_2 \approx 5\ \mu m \quad (26)$$

4.2. *Using High–Rate Mode Data*

Here we shall use the high–rate mode data to estimate the exponent p of the dust mass distribution.

As described in section 2.1, a high–rate mode frame (48 s), which was acquired in the 308.4– and 615.6–kHz channels at the time labelled P in Figures 3*a* and 3*b* ($\sim$0513 SCET), i.e., about 3 min before the maximum density of the outbound crossing, shows clear signatures of individual grain impacts.

An extract of this frame is displayed in Figure 3*c*. Due to the much shorter integration time $\Delta t_{hr} \approx 100$ μs, compared to the one for the routine data, we can discern the individual impacts, although as $\tau_r < \Delta t_{hr}$, we cannot resolve correctly the rising part of the voltage. The impact rate during this time interval is found to be

$$N \approx 65\text{ s}^{-1}$$

In order to use this result in a meaningful way we must recall that with usual dust distributions (satisfying $p > 1$), the impact rate N (equation (10)) is determined by the smallest detected grains, i.e., by the sensitivity of the receiver. An estimate of the pulse height due to a grain of mass m in the high–rate mode at frequency f is, instead of (7),

$$E_{hr}^2 \approx 2q^2 m^{1.6}/L^2 C_0^2 \tau_r^2 \Delta t_{hr} (2\pi f)^4 \quad (27)$$

$$E_{hr}^2 \approx 4.3 \times 10^{24} m^{1.6}/f^4 \quad (28)$$

where, as previously, the f^{-4} variation stems from the rise part of the signal which still satisfies $2\pi f \tau_r >> 1$.

With the sensitivity $E_{min}^2 \approx 6 \times 10^{-17}$ V^2 m^{-2} Hz^{-1} we deduce the minimum detected mass in the high-rate mode at $f = 6 \times 10^5$ Hz, in grams

$$m_1 \approx \left(\frac{E_{min}^2 \Delta t_{hr} L^2 C_0^2 \tau_r^2 (2\pi f)^4}{2q^2} \right)^{1.6} \quad (29)$$

By using the level of the power spectrum for the routine data mode around the same time we can deduce the exponent p. Since the two PRA modes cannot be operated simultaneously, the power spectrum in the routine mode has not been measured at the time when we have an estimate of N, but we can evaluate it by interpolating between values just before and after the high-rate sequence. This gives a level E^2 about 250 times smaller than the one of the maximum density at the outbound crossing, given in (17). Then from (18) we deduce that the largest grains that would be detected in the routine mode at this time have a mass

$$m_2 \approx \left(\frac{2 \times 10^7 \Delta t L^2 C_0^2 \tau_r^2 (2\pi)^4}{250 \times 2q^2} \frac{2.6 - p}{p - 1} \right)^{1/1.6}$$

Using the expressions for m_2 (13) and m_1 (29) and eliminating A by using (10), we get

$$(m_2/m_1)^{p-1} = N \Delta t \quad (30)$$

$$(m_2/m_1)^{p-1} = \left(\frac{2 \times 10^7 \Delta t}{250 f^4 E_{min}^2 \Delta t_{hr}} \frac{2.6 - p}{p - 1} \right)^{(p-1)/1.6} \quad (31)$$

thus

$$1.6 \approx 1.8^{p-1} \left(\frac{2.6 - p}{p - 1} \right)^{(p-1)/1.6}$$

from which we deduce $p \approx 1.8$. Note that this value must be taken with much caution in view of the uncertainties involved.

We can now check this result by using an independent and perhaps more reliable estimate. Figure 5 shows a histogram of the distribution of the observed pulses in the high-rate mode. Since we have $E_{hr}^2 \propto m^{1.6}$, the number of pulses with amplitude larger than E_{hr}^2 varies as E_{hr}^2 at the power $(1 - p)/1.6$; thus the slope of the histogram giving the number of pulses in each bin of log E_{hr}^2 is $(1 - p)/1.6$. From Figure 5 we deduce the value $p \approx 2$.

4.3. *Dust Mass Distribution*

Hence we have for p the approximate value

$$p \approx 2 \quad (32)$$

around 0513 SCET, i.e., around 4.2 R_N. This corresponds to a size distribution $dn_G/da \propto 1/a^{3p-2} \propto 1/a^4$.

Let us assume that p does not vary significantly during the outbound ring plane crossing. This allows us to deduce the amplitude A of the distribution at its maximum value. From (26) we get $m_2 \approx 4 \times 10^{-10}$ g. Thus with the aid of (13) we get

outbound (4.26 R_N)

$$A \approx 7 \times 10^{-14} \quad (33)$$

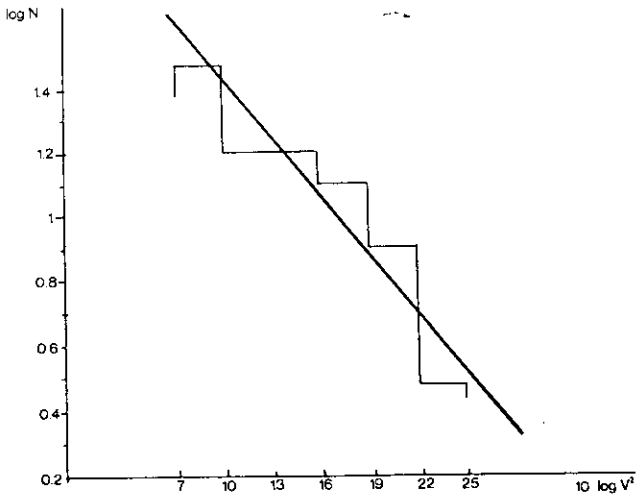

Fig. 5. Logarithmic histogram of individual grain impacts from high-rate mode frame, recorded before the second ring plane crossing: The number of events in a given intensity range is plotted as a function of intensity. The heavy line corresponds to the power law index $p = 2$.

With (22) we get for the number density (in units per cubic meter) of grains larger than a given mass m (in grams)

$$n_{G>m} \approx 7 \times 10^{-14}/m \quad (34)$$

As an example, the number density of grains larger than 4×10^{-12} g ($a = 1$ μm) is about 2×10^{-2} m^{-3} at the maximum density of the outbound crossing.

If we assume that the exponent p is the same at the inbound crossing, we get in the same way from (25) $m_2 \approx 4 \times 10^{-9}$ g. Thus with the aid of (13),

inbound (3.45 R_N)

$$A \approx 7 \times 10^{-13} \quad (35)$$

Again with (22) we get for the number density of grains larger than a given mass m (in grams)

$$n_{G>m} \approx 7 \times 10^{-13}/m \quad (36)$$

For instance, the number density of grains larger than 4×10^{-12} g ($a = 1$ μm) is about 0.2 m^{-3} at the maximum density of the inbound crossing.

4.4. *Dust Spatial Distribution*

We can also get a tentative estimate of the spatial distribution of the grains. Let us still assume that the grain mass distribution has the form given in (9) with the value $p = 2$ previously estimated. From (13) and (14) we know that the level of the electric field power spectrum varies as $E^2 \propto A^{1.6}$. Thus the observed variation of E^2 gives the spatial variation of the grain number density as

$$A \propto \left(E^2\right)^{1.6} \quad (37)$$

From the ephemeris at the equatorial plane crossings (A. Lecacheux, private communication, 1990) we find the following expressions for the spacecraft velocity in a Neptune-centered (but not rotating) coordinate system, presented in cylindrical coordinates with the z axis perpendicular to Neptune's equatorial plane and ρ and θ referring to radial and azimuthal directions in this plane:

inbound

$$v_\rho \approx -18.8 \text{ km/s},$$
$$v_\theta \approx -2.8 \text{ km/s},$$
$$v_z \approx 9.1 \text{ km/s}$$

outbound

$$v_\rho \approx 18.7 \text{ km/s},$$
$$v_\theta \approx -2.6 \text{ km/s},$$
$$v_z \approx -7.5 \text{ km/s}$$

The observed variation of E^2 with the spacecraft location has several components. First, we see a weak noise, mostly visible in the lowest-frequency channels, that extends (in the 1.2-kHz channel) from about 0140 to 0330 SCET, i.e., about 70 min before to 40 min after the inbound crossing, and from 0450 to 0600 SCET, i.e., about 25 min before to 45 min after the outbound crossing. Translated into spatial distances, this corresponds to a diffuse dust layer labeled "halo" in Figure 6. It extends at least from 1.6 to 6.5 R_N in the equatorial plane during the inbound path and from 3 to 6.2 R_N during the outbound path, with a width nearly 2 R_N in the z direction. Since this component is barely visible except in the 1.2-kHz channel, its theoretical interpretation is not straightforward, as it may be due to grains passing near the spacecraft without impacting it [*Meyer-Vernet*, 1991], and for the time being we do not try to deduce the corresponding grain mass and concentration.

We shall now analyze the main components, whose maxima near the ring plane crossings were studied in sections 4.1 and 4.3. Far from the ring plane, when the intensity level is lower, the spectra become less steep, decreasing somewhat more slowly than f^{-4} at high frequencies. Since the signal is rather low at these high frequencies, it might be contaminated by other emissions, so that we will use mostly the low-frequency channels to study the spatial variations.

First, we analyze the inbound crossing (see Figure 2). We note that the maximum of the noise is at 0253:10 ± 10 s SCET, thus about 18 s after the equatorial plane crossing, which occurs at 0252:52 SCET (this shift corresponds to 400 km along the spacecraft trajectory). The spectra are very noisy, as can be expected, since the level depends on the mass, raised to the power 1.6, of the largest grain which has impacted during the integration time. So it is difficult to deduce a precise law of variation. In order to estimate a meaningful scale length we will assume that the grain concentration varies in a Gaussian way with the distance along the trajectory; note that this is merely a convenient but unproved assumption, although it is compatible with our data. The grain concentration is directly proportional to the parameter A in (9) if the mass power law index p remains the same. From (37) a variation with the time t,

$$A \propto \exp -(t-t_0)^2/\delta t^2 \tag{38}$$

translates into $E^2 \propto \exp -1.6\,(t-t_0)^2/\delta t^2$. From the observed variation we thus deduce $\delta t \approx 31$ s, which corresponds to a distance along the spacecraft trajectory (at ~21 km/s) of 650 km.

Without additional assumptions we cannot deduce a three-dimensional grain spatial distribution. But since the grain concentration is maximum near the equatorial plane, it may be a plausible assumption that the variations observed along the spacecraft trajectory are due mostly to the variation of the distance z to this plane, which means that the grain concentration varies more slowly with ρ and θ (i.e., within the equatorial plane) than with z.

Thus, assuming

$$A = A_0 \exp -(z-z_0)^2/\delta z^2 \tag{39}$$

we have (with $v_z = 9$ km/s) $z_0 = 160$ km and $2 \times \delta z = 560$ km. This corresponds to a dust layer with maximum concentration at about 160 km above the equatorial plane, at a distance 3.45 R_N from Neptune, and with a vertical thickness 560 km.

However, it is important to note that the observed variation might also be due to a variation of the concentration with the radial distance (or, but less plausibly, with θ). Furthermore, the observed shift of the maximum with respect to the equatorial plane crossing might be due to an error in the ephemeris. Indeed, the ephemeris that we have used depends on the determination of the planetary rotation pole, whose most recent value, as calculated from Voyager imaging results [*Nicholson et al.*, 1990], has angular errors of order 0.1°. This corresponds to about

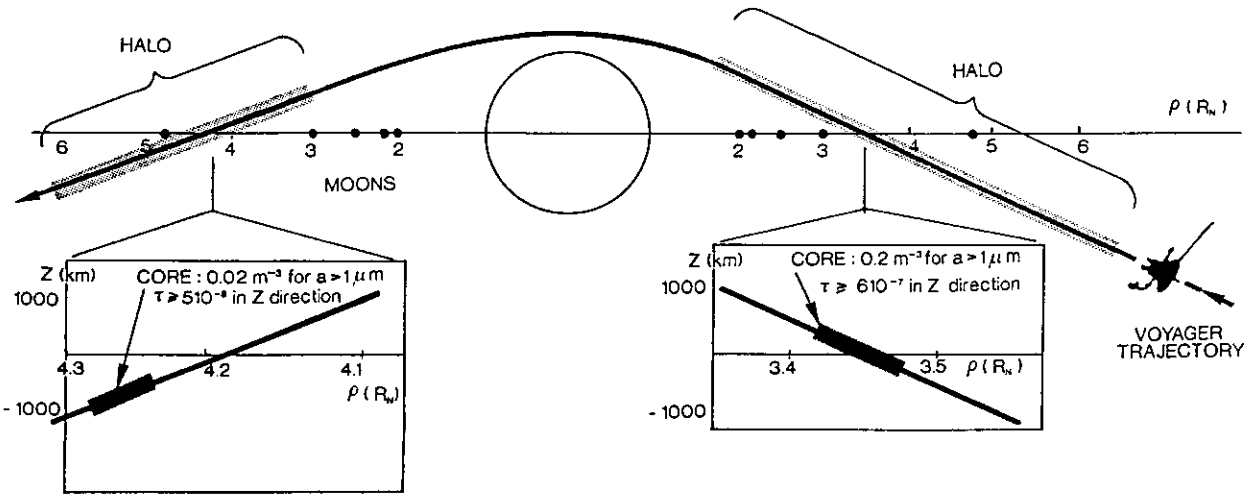

Fig. 6. Schematic illustration of the dust distribution as deduced from our study. The light gray areas diplay the halo, i.e., the extended low-density region observed with the 1.2-kHz channel. Insets show details of the spacecraft trajectory in the vicinity of the equatorial plane crossings; regions with largest measured densities are shown as dark gray areas. Corresponding densities and optical depths are indicated.

140 km at 3.45 R_N, and is thus of the same order as the observed shift z_0.

We now estimate the corresponding vertical optical depth τ and mass column density σ. With the mass distribution (9) we have

$$\tau = \int_{-\infty}^{+\infty} dz \int da\, Q_{ef}(a)\, \pi a^2 dn_G/da = \sqrt{\pi}\delta z \left(3\sqrt{\pi}/4d\right)^{2/3} A_0 \int_{m_{min}}^{m_{max}} dm\, m^{2/3-p}$$

$$\sigma = \int_{-\infty}^{+\infty} dz \int dm\, m\, dn_G/dm = \sqrt{\pi}\delta z A_0 \int_{m_{min}}^{m_{max}} dm\, m^{1-p}$$

where we have set, for making an order of magnitude estimate, the extinction efficiency $Q_{ef} = 1$; m_{min} and m_{max} are the mass of the smallest and largest relevant grains, respectively, and d is their mass density. We obtain, with $p = 2$ and $m_{min} \ll m_{max}$ (in SI units),

$$\tau = 6{\cdot}4\, A_0 \delta z / \left(d^{2/3} m_{min}^{1/3}\right) \quad (40)$$

$$\sigma = \sqrt{\pi}\, A_0\, \delta z \ln(m_{max}/m_{min}) \quad (41)$$

With $d = 1$ g/cm^3 and A_0 determined in (35) (and transformed into convenient units), we get

$$\tau \approx 1.2 \times 10^{-10}/m_{min}(\mathrm{g})^{1/3} \quad (42)$$

$$\sigma \approx 3.5 \times 10^{-11} \ln(m_{max}/m_{min}) \quad \mathrm{g/cm^2} \quad (43)$$

We do not know m_{min} and m_{max}. But we can assume that m_{min} is smaller than or equal to the smallest mass m_1 detected and that m_{max} is larger than or equal to the largest mass m_2 that we have detected around the inbound crossing. Thus using (29) which gives $m_1 \approx 8 \times 10^{-12}$ g (1.6 μm grains), and (25), we obtain

$$\rho^{\mathrm{inbound}} \approx 3.45\ R_N \qquad \tau \geq 6 \times 10^{-7} \quad (44)$$

$$z_0 \approx 160\ \mathrm{km} \qquad \sigma \geq 2 \times 10^{-10}\ \mathrm{g/cm^2} \quad (45)$$

In order to study the outbound ring plane crossing (Figure 3*b*) we first note that the maximum of the noise that we have studied in sections 4.1 and 4.3 occurs at 0516:10 $\pm$10 s SCET, thus about 94 s later (i.e., 1940 km along the spacecraft trajectory) than the outbound equatorial plane crossing, which occurs at 0514:36 SCET. Translated into spatial distances, this time delay corresponds to a shift $\rho - \rho_0 \approx 1800$ km in radial distance and a location $z_0 \approx -700$ km below the equatorial plane (and about 250 km in the azimuthal direction).

As previously, we cannot deduce unambiguously the three-dimensional dust distribution. A shift from the equatorial plane might be due to an actual asymmetry of the dust concentration with respect to the equatorial plane and/or a nonuniformity of the dust concentration in the equatorial plane (either in ρ or θ), or (less plausibly) it might be due to an unexpected error in the ephemeris.

Assuming as previously a Gaussian variation of the concentration and $p = 2$, we find a half width about the same as in the inbound crossing, i.e., $\delta t \approx 31$ s. This corresponds to widths $2 \times \delta\rho \approx 1200$ km and $2 \times \delta z \approx 460$ km.

Now we can estimate the corresponding optical depth and mass column density integrated along the z coordinate. By using (33) and (26), we find

$$\rho^{\mathrm{outbound}} \approx 4.26\ R_N \qquad \tau \geq 5 \times 10^{-8} \quad (46)$$

$$z_0 \approx -700\ \mathrm{km} \qquad \sigma \geq 10^{-11}\ \mathrm{g/cm^2} \quad (47)$$

5. RELIABILITY OF THE RESULTS

A few comments are in order. The PRA experiment, like the other investigations aboard Voyager, was not optimized to detect dust grains. Indeed, at the time of Voyager launch it was not anticipated that this experiment would serve as a dust detector. As a result we have been obliged to use the results in an unusual way and to make many working hypotheses as to the response of the experimental setup to dust impacts; so one could have legitimate doubts about the reliability of the results.

A major problem is that the charge Q re-collected as a function of the grain mass is poorly known, as discussed in section 3.1: the parameter q in (5) is uncertain, and the actual variation of Q might be different from $m^{0.8}$; furthermore, the rise time τ_r of the signal induced by an impact is not precisely determined (in comparison, the uncertainty regarding the relevant spacecraft surface for dust impacts is not important). Among those uncertainties the major one is that regarding q; indeed, it depends on the incident velocity v to the power 3.5, and our estimate of v relies on the assumption that all the grains are moving in direct Keplerian rotation in Neptune's rotational equatorial plane, which is by no means certain; in addition, q also depends on the grain's physical and chemical state and also on the spacecraft response, which are all unknown. As a consequence we believe that our estimates of dust number densities (which vary as q^2, multiplied by the total relevant projected surface) might be off by a factor of 100.

Another problem is that because the electric power spectrum is proportional to an integration over $m^{1.6}$, an independent knowledge of the grain mass distribution is necessary to fully interpret the results. In order to get this independent estimate we have used data in a high-rate mode, which were obtained about 700 km from the ring plane. Thus we have assumed that the distribution has a single power law form $\propto m^{-p}$ in the relevant mass range with an exponent p being constant over this distance; this assumption is not necessarily true, since lighter grains being more sensitive to electromagnetic forces, are more likely to reside outside the ring plane. In order to get a more reliable result, however, we have determined p by two independent methods. We have also verified that changing the exponent p (from 2 to 1.5, for instance) would not change the overall results too much.

The above uncertainties might also affect our estimates of the dust spatial distribution, if the nature or velocity of the grains or the exponent of their mass distribution is not constant over the core of the dust layer.

6. WHAT HAVE WE LEARNED ABOUT NEPTUNE'S DUST GRAINS?

As discussed by *Smith et al.* [1989] and *Colwell and Esposito* [1990], the Neptunian ring system is relatively dusty. Sources of dust may be due to meteoroid impacts onto moons and large ring particles and to collisions between ring particles which release regolith material. *Colwell and Esposito* [1990] use a model with ring dust particles in the size range 0.1 to 2 μm, which contains most of the dust optical depth.

In this paper we have studied the dust grains outside this ring system, in the vicinity of Voyager 2's two consecutive crossings of Neptune's equatorial plane (at $\sim$3.4 R_N and $\sim$4.2 R_N). The electric field density spectrum associated with both crossings has been interpreted in terms

of grain impacts. Because the high-rate mode data show that the impacting particles are not identical, we have assumed that the impacting grains have a continuous mass distribution of the form $dn_G/dm = Am^{-p}$. From the high-rate mode data we get for the outbound crossing an estimate of the exponent $p \approx 2$. This corresponds to a size distribution $dn_G/da \propto a^{-4}$. For such a continuous distribution the recorded power is sensitive to the largest grains, whereas the impact rate (and the related optical depth) is sensitive to the smallest ones. The largest detectable grains (assuming solid water ice spheres), i. e., those for which the probability of impacting during the PRA routine measuring time $\Delta t = 25$ ms is not negligible, during inbound and outbound ring plane crossings have radii of 10–13 μm and $\sim$5 μm, respectively. On the other hand, we show that the PRA system is sensitive to grains with radii larger than $\sim$1.6 μm.

At the maximum density of the two equatorial crossings we find for the number density (in units per cubic meter) of grains larger than a given mass m (in grams)

outbound

$$n_{G>m} \approx 7 \times 10^{-14}/m$$

and assuming the same value of the exponent $p = 2$,

inbound

$$n_{G>m} \approx 7 \times 10^{-13}/m$$

For example, the number density of grains larger than 4×10^{-12} g ($a \geq 1$ μm) is about 0.02 m^{-3} and 0.2 m^{-3} at the maximum density of outbound and inbound crossings.

Figure 6 schematizes the spatial dust distribution, as deduced from our observations. A weak noise component, only observable in the lowest PRA channel (1.2 kHz), is interpreted as a diffuse dust layer (labeled "halo" in Figure 6). It is spread at least from 1.6 to 6.5 R_N in the equatorial plane during the inbound path and from 3 to 6.2 R_N during the outbound path and extends over about 2 R_N in the perpendicular direction.

The core of the dust distribution near the equatorial plane is deduced from the emissions at higher frequencies as described in section 4.4. For the inbound crossing at 3.45 R_N we observe a 650-km-long density enhancement along the spacecraft trajectory, corresponding to a dust layer with maximum concentration at about 160 km above the equatorial plane with a vertical thickness of 560 km. This corresponds to an optical depth in the z direction $\tau \geq 6 \times 10^{-7}$ and a mass column density $\sigma \geq 2 \times 10^{-10}$ g/cm^{-2}.

The corresponding emission during the outbound path was detected along 1940 km of the spacecraft trajectory, although considerably shifted with respect to the equatorial plane crossing at 4.26 R_N. The shift corresponds to a outward radial displacement of $\sim$1800 km and a location of $\sim$700 km below the plane (and about $\sim$250 km in azimuthal direction). This corresponds to a vertical optical depth $\tau \geq 5 \times 10^{-8}$ and a mass column density $\sigma \geq 10^{-11}$ g/cm^{-2}.

These optical depths are too small to be easily observed by the Voyager imaging experiment. Likewise, the mass column densities are very small, so that detecting an absorption of the energetic electrons and ions, measured in situ on board Voyager, is not a simple matter.

Whereas the small shift of the location of the detected maximum density with respect to the inbound equatorial crossing is probably not significant, the much more important shift observed during the outbound path may be real (assuming that the ephemeris we have used is correct). However, we cannot sufficiently dissuade anyone from jumping prematurely to the conclusion that we have detected a dust layer, tilted from the equatorial plane, curled, or whatever, even if such a situation may seem interesting for a theorist, owing to the large variety of forces at work on the grains. But after all, the Voyager flyby has only provided us with a unique set of measurements along the spacecraft trajectory, and not a three-dimensional distribution.

Acknowledgments. We thank A. Lecacheux for constructive discussions and for having communicated spacecraft trajectory and attitude data. Thanks are also due to E. C. Sittler, Jr., and J. W. Belcher from the Voyager PLS team for having allowed us to use preliminary ring plane plasma parameters and to M. H. Acuna for providing informations concerning the surface materials of the Voyager spacecraft.

The editor thanks two referees for their assistance in evaluating this paper.

REFERENCES

Aubier, M. G., N. Meyer-Vernet, and B. M. Pedersen, Shot noise from grain and particle impacts in Saturn's ring plane, *Geophys. Res. Lett., 10*, 5–8, 1983.

Colwell, J. E., and L. W. Esposito, A model of dust production in the Neptune ring system, *Geophys. Res. Lett., 17*, 1741–1744, 1990.

Göller, J. R., and E. Grün, Calibration of the Galileo/Ulysses dust detector with different projectile materials and at varying impact angles, *Planet. Space Sci., 37*, 1197–1206, 1989.

Grün, E., H. A. Zook, H. Fechtig, and R. H. Giese, Collisional balance of meteoritic complex, *Icarus, 62*, 244–272, 1985.

Gurnett, D. A., et al., Micron-sized particles detected near Saturn by the Voyager plasma wave instrument, *Icarus, 53*, 236–254, 1983.

Gurnett, D. A., et al., Micron-sized particle impacts detected near Uranus by the Voyager 2 plasma wave instrument, *J. Geophys. Res., 92*, 14,959–14,968, 1987.

Gurnett, D. A., et al., First plasma wave observations at Neptune, *Science, 246*, 1494–1498, 1989.

Kruger, F. R., and J. Kissel, Experimental investigations on ion emission with dust impact on solid surfaces, The Giotto Spacecraft Impact-Induced Plasma Environment, Eur. Space Agency Spec. Publ., *ESA SP 224*, 43, 1984.

Lesceux, J. M., J. Lemaire, and N. Meyer-Vernet, Electric dipole antennae used as micrometeoroid detector, *Planet. Space Sci., 37*, 1291–1302, 1989.

Meyer-Vernet, N., Electrostatic noise generated by dust grains moving in an equilibrium plasma, Space Simulation, Radio Atmos. Sci. Cent., Kyoto Univ., Kyoto, Japan, 1991.

Meyer-Vernet, N., and C. Perche, Tool kit for antennae and thermal noise near the plasma frequency, *J. Geophys. Res., 94*, 2405–2415, 1989.

Meyer-Vernet, N., M. G. Aubier, and B. M. Pedersen, Voyager 2 at Uranus: Grain impacts in the ring plane, *Geophys. Res. Lett., 13*, 617–620, 1986.

Nicholson, P. D., M. L. Cooke, K. Matthews, J. H. Elias, and G. Gilmore, Five stellar occultations by Neptune: Further observations of ring arcs, *Icarus, 87*, 1–39, 1990.

Smith, B. A., et al., Voyager 2 at Neptune: Imaging science results, *Science, 246*, 1422–1449, 1989.

Warwick, J. W., J. B. Pearce, R. G. Peltzer, and A. C. Riddle, Planetary radio astronomy experiment for Voyager missions, *Space Sci. Rev., 21*, 309–327, 1977.

Warwick, J. W., et al., Voyager planetary radio astronomy at Neptune, *Science, 246*, 1498–1501, 1989.

M. G. Aubier, Université de Paris VI and CNRS URA 324, Observatoire de Paris–Meudon, 92195 Meudon Principal Cédex, France.

N. Meyer-Vernet, CNRS URA 264, Observatoire de Paris–Meudon, 92195 Meudon Principal Cédex, France.

B. M. Pedersen and P. Zarka, CNRS URA 324; Observatoire de Paris–Meudon, 92195 Meudon Principal Cédex, France.

(Received January 4, 1991;
revised June 10, 1991;
accepted June 11, 1991.)